crystals

MDPI

Article

Morphology and FTIR Characteristics of the Alluvial Diamond from the Yangtze Craton, China

Chuqi Cao [1], Jingsui Yang [1,2,3,*], Fengshan Zeng [4], Fei Liu [1,3], Shengbiao Yang [1] and Yun Wang [2]

[1] Institute of Geology, Chinese Academy of Geological Sciences, Beijing 100037, China; chuqicao@163.com (C.C.); liufei@cags.ac.cn (F.L.); shbyang@163.com (S.Y.)
[2] School of Earth Sciences and Engineering, Nanjing University, Nanjing 210023, China; ewangyun@163.com
[3] Shandong Academician Workstation of Diamond Mineralization Mechanism and Exploration, Shandong No. 7 Exploration Institute of Geology and Mineral Resources, Linyi 276006, China
[4] Hunan Urban Geological Survey and Monitoring Institute, Changsha 410000, China; dzb414@126.com
* Correspondence: yangjsui@163.com

Abstract: A total of 48 natural alluvial diamonds from the Yangtze Craton, China, also called Hunan diamonds, were studied using morphology and IR spectroscopy. These diamond samples, collected downstream of the Yuan River, Hunan Province, with unknown host-rock source(s), were observed by scanning electron microscope (SEM) and Fourier-transform infrared spectroscopy (FTIR). Most Hunan diamonds are monocrystal forms of octahedra, tetrahexahedra (THH) and dodecahedra; octahedral–rhom-dodecahedral transitional behaviors and irregular forms are also visible. Trigons and tetragons, terraces and shield-shaped laminae are surface features that frequently indicate dissolution and reabsorption; green and brown spots, network patterns, and other mechanical abrasion marks are typical evidence of long-time deposition and transportation of Hunan diamonds. The main types of Hunan diamonds are type IaAB and type IIa. Diamond samples have a wide range of total nitrogen content (N_{tot}) from 196–1094 ppm. Two populations are distinguished by two-peak distribution models of N_A (A-center concentrations) and %B (proportion of aggregated nitrogen). Hunan diamonds are low in structure hydrogen (0.03–4.67 cm^{-1}, mostly below 1 cm^{-1}) and platelets (0.23–17 cm^{-1}, mostly below 2 cm^{-1}). Moreover, there is a significant positive correlation between the hydrogen correlation peak and N_{tot}, which is similar to Argyle diamonds. The temperature conditions of the diamond formation have been estimated at 1075–1180 °C, mainly conforming to the kimberlite diamond range. Besides, some samples with slightly higher temperatures are close to the ultramafic-related Juina diamonds. Therefore, the FTIR characteristics analysis and comparison indicate the multiple sources of Hunan diamonds.

Keywords: alluvial diamond; morphology; FTIR; nitrogen; hydrogen; temperature

Citation: Cao, C.; Yang, J.; Zeng, F.; Liu, F.; Yang, S.; Wang, Y. Morphology and FTIR Characteristics of the Alluvial Diamond from the Yangtze Craton, China. *Crystals* **2022**, *12*, 539. https://doi.org/10.3390/cryst12040539

Academic Editor: Giuseppe Prestopino

Received: 26 February 2022
Accepted: 5 April 2022
Published: 12 April 2022

1. Introduction

Most natural diamonds from the earth's mantle and are transported to the surface by deep mantle magmas, such as kimberlites and lamproites [1]. Nitrogen and hydrogen are the most common impurity elements in natural diamonds, and diamonds are primarily classified on the basis of nitrogen-containing defects in the crystal lattice.

Fourier-transform infrared spectroscopy (FTIR) provides a method for estimating the concentration of nitrogen defects (A-center and B-center), hydrogen centers (H), and "Platelets" (P) [2]. It is one of the most widely used methods for investigating the state of structural nitrogen-bearing aggregates in diamonds and identifying diamond types [3–6].

The high refractive index of diamond makes optical microscopy a powerful tool to study diamond surface features and crystal morphology. Optical microscopy is sufficient for discriminating diamonds with kimberlite-induced and mantle-derived resorption [7], for identification of resorption by fluid-rich and fluid-poor kimberlite magmas, and resorption types from different events of mantle metasomatism [8].

Scanning electron microscopy (SEM) is a practical approach to observe the details of surface features on complicated diamond crystals both in secondary electrons (SEs) and backscatter electrons (BSEs) [9].

There are rich alluvial-diamond placers in the Yangtze Craton, China, in which sub-rounded and rounded diamonds coexist with indicator minerals (pyrope, Mg ilmenite, and chromite) [10], similar to some famous diamond-placer deposits in the eastern Siberian craton, the Urals, Africa, etc. The Yuan River basin in the Yangtze Craton is a significant source of alluvial diamonds discovered in China. Several diamondiferous placer deposits have been identified at each reach of the Yuan River basin, yielding diamond crystal grains that are mostly macro-diamond monocrystals of good quality [11].

Some examinations by morphology, IR spectroscopy and isotope analyses have led to the conclusion that the original host rocks of diamonds in the Yuan River basin are kimberlite or lamproite [12]. Still, the primary deposits of these alluvial diamonds have not yet been identified. Thus, the research on morphologic and FTIR spectral characteristics of diamonds from the Yangtze Craton must be continued. In this study, new experimental data and discussions based on SEM and FTIR about aspects of morphology, structural nitrogen and hydrogen defects provide a better understanding of diamond-formation conditions and temperature parameters at the source of the alluvial diamond from the Yangtze Craton.

2. Geological Setting

The Yangtze Craton is situated in south China over an area of 1,400,000 km^2, and is the second-largest cratonic block in China [13] (Figure 1a). The Yangtze Craton is bordered on the southeast by the Jiangnan orogen, to the north by the Qinling–Dabie–Sulu orogen, to the west by the Songpan–Ganzi terrane, and to the southwest by the Jinshajiang–Ailaoshan–Song Ma suture zone [13,14]. The assembly of the Yangtze Craton formed in the Archean period with an Archean–Paleoproterozoic crystalline basement [15] and has a crustal remnants as old as 3.8 Ga [15,16]. The Yuan River within the Yangtze Craton originates from the Miao Mountains in Guizhou Province, ultimately discharging into the Dongting Lake in Hunan Province, with a total length of 864 km [12]. The Yuan River with its Cretaceous continental red beds is the most important source of alluvial diamonds in China. Since the 1950s, a series of diamond placers have been discovered in the regions of Zhenyuan, Chenxi, Changde and Huaihua within the Yuan River basin (Figure 1b) [12]. Several outcrops or rock debris of kimberlites and lamproites containing small amounts of diamonds have been identified (Figure 1b) in Zhenyuan, Changde [12,17,18], while no primary diamond deposit has been found so far. The Hunan diamond samples investigated in this study were collected by the mineral-processing test during diamond prospecting in the Changde region in the lower reaches of the Yuan River basin.

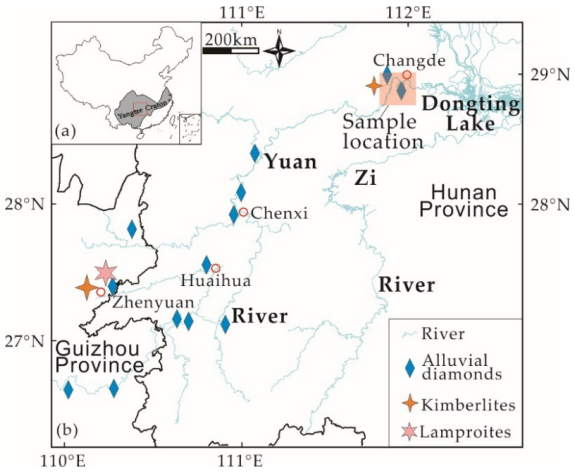

Figure 1. (**a**) Location map for the Yangtze Craton; (**b**) Sketch map of the Yuan River basin and the sample location. Modified by [12].

3. Materials and Methods

A total of 48 rough diamond samples collected from the Yuan River basin, Hunan Province, China, were studied. The diamonds labeled by the sample number from HN001 to HN048, also called "Hunan Diamond", were all monocrystal diamonds, with sizes ranging from 1.2–9.6 mm and weights varying from 1.1–177 mg.

The properties of the diamond samples were observed and photographed, studied by SEM and FTIR spectrometry.

Initial observation and photography of the samples were performed on a Zeiss Stemi 508 optical stereo microscope at the Chinese Academy of Geological Sciences.

SE and BSE photographs of diamond samples were obtained simultaneously at the Geological Institute of the Chinese Academy of Geological Sciences using an FEI Quanta 450 SEM operating at 20 kV and a beam current of 15 nA.

Before FTIR testing, each diamond sample was cleaned with a 40 KHz ultrasonic cleaner for 5 min to remove clay and stains adhering to the crystal surface in order to avoid IR absorption peaks of impurities from interfering with the test results.

The FTIR spectra were measured by a Bruker LUMOS FTIR spectrometer with transmission mode at the School of Gemology, China University of Geosciences (Beijing). The recording was made at local surface points of crystals in the region 4000–600 cm^{-1}, resolution of 4 cm^{-1}, and more than 32 scans. Each sample was tested multiple times at different locations on the surface. The spectrogram records revealed 41 diamond samples in which the nitrogen content and aggregation state did not vary along with the crystal profile or vary negligibly. The other 7 diamond samples did not show a valid infrared spectrum in the tests, possibly due to the lack of flatness of the crystalline surface.

To determine the absorption coefficients of the 41 differently sized diamonds in the IR region, the measured spectra were baseline corrected and normalized to an effective thickness of 1 cm by an absorption coefficient of 13 absorption unit/cm^{-1} at 2030 cm^{-1} [19–21]. The absorption spectrum had a resolution of 1 cm^{-1}.

The nitrogen content of A- and B-centers in terms of at. ppm was calculated from the absorption peaks at the frequencies of 1282 cm^{-1} and 1175 cm^{-1} [4,5,22]. The relative error in nitrogen concentration appeared to be $\pm$10 to 20%.

The relative proportions of "Platelets" (B′-defects) and hydrogen (H) structural impurities in diamonds were estimated by the absorption strengths of absorption-coefficient values at 1360–1370 cm^{-1} and 3107 cm^{-1}, respectively [23].

4. Results and Discussion

4.1. Morphology

Natural diamonds exist in various shapes that reflect growth under different conditions of supersaturation and resorption [24,25]. Diamond morphology in alluvial deposits reflects the conditions of crystal growth and provides information on the process of diamond formation [25]. Typical crystal forms and surface features associated with dissolution and reabsorption in diamond samples will be discussed, while features related to transportation and mechanical abrasion that alluvial diamonds endured such as spots and network patterns are also identified and labeled.

4.1.1. Crystal Form

In this study, we use dodecahedra to describe diamonds with 12 curved faces that are formed when the {111} face resorbs via formation of the trigonal shape, and tetrahexahedra (THH) to describe the rounded diamonds with 24 curved faces [26–28], which develop when the initial octahedral {111} face resorbs via formation of the ditrigonal shape [27]. Diamonds with octahedral growth morphology and their transition into tetrahexahedra (THH) or dodecahedra due to dissolution are shown in Figure 2a.

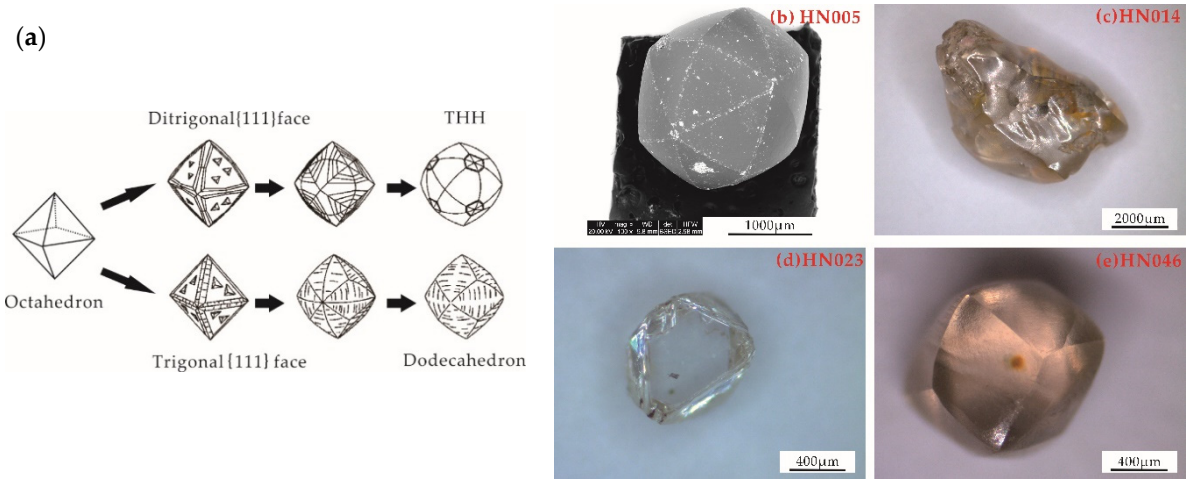

Figure 2. (**a**) Evolution of diamond crystal morphology due to resorption from octahedron to tetrahexahedron (THH) or dodecahedron forms via development of ditrigonal or trigonal shape of {111} faces, respectively (modified after [26,27]); The photographs (**b**–**e**) showing classical crystal forms of the alluvial diamonds from the Yangtze Craton: (**b**) Tetrahexahedra (THH); (**c**) Irregular form; (**d**) Octahedra; (**e**) Dodecahedra.

The common monocrystal forms observed in Hunan diamond samples (e.g., Figure 2b) are octahedra, tetrahexahedra (THH) and dodecahedra. Additionally, octahedral–rhom-dodecahedral transitional behaviors and irregular forms were also present among the samples. No twin crystals were observed in these samples.

4.1.2. Trigons and Tetragons

Trigons are typically present on the {111} diamond faces in octahedral-shaped diamonds [29]. Tetragons usually occur on the cubic {100} diamond faces and rarely on octahedral diamonds, but in some kimberlite-hosted diamonds, tetragons can become a common feature on THH diamonds, where they develop in the crystal apices and on positively-oriented walls of hexagonal pits [9]. It has been accepted that trigons and tetragons are dissolution and resorption features that are related to the effect of kimberlite magma or mantle metasomatism on the diamond surface [9,30].

Trigonal pits are considered to be positive if they are aligned in the same orientation as the octahedral diamond edges (Figure 3b) and negative if the orientation of the apices of the etch pits and the octahedron faces differ by 180° (Figure 3a). Initially, the pits were small pyramidal forms, and continued resorption increased their width and flattened their bases. Aggregations of small shallow trigonal etch pits may be derived from the etching of near-surface micro-defects [31,32].

Positive trigons are rare on natural diamonds [28,33]. Since the resorption by kimberlite magma would have affected a larger proportion of the diamond population, the rare and unusual positively oriented trigon features may point towards an exotic mantle event and rare late resorption [9,34].

Tetragonal etch pits are dissolution features that form in the same way as trigons [9]. Additionally, similarly to trigonal etch pits, tetragonal etch pits can exhibit positive or negative orientations, e.g., sample HN044 contains negatively-oriented tetragonal pits with edge lengths between 10–100 μm with a "pyramidal shape" (Figure 3c).

4.1.3. Terraces

Terraces typically evolve from fine parallel lines outlining around the crystal apices of dodecahedra (Figure 3d). These features are called terraces [28] or striations [8,26].

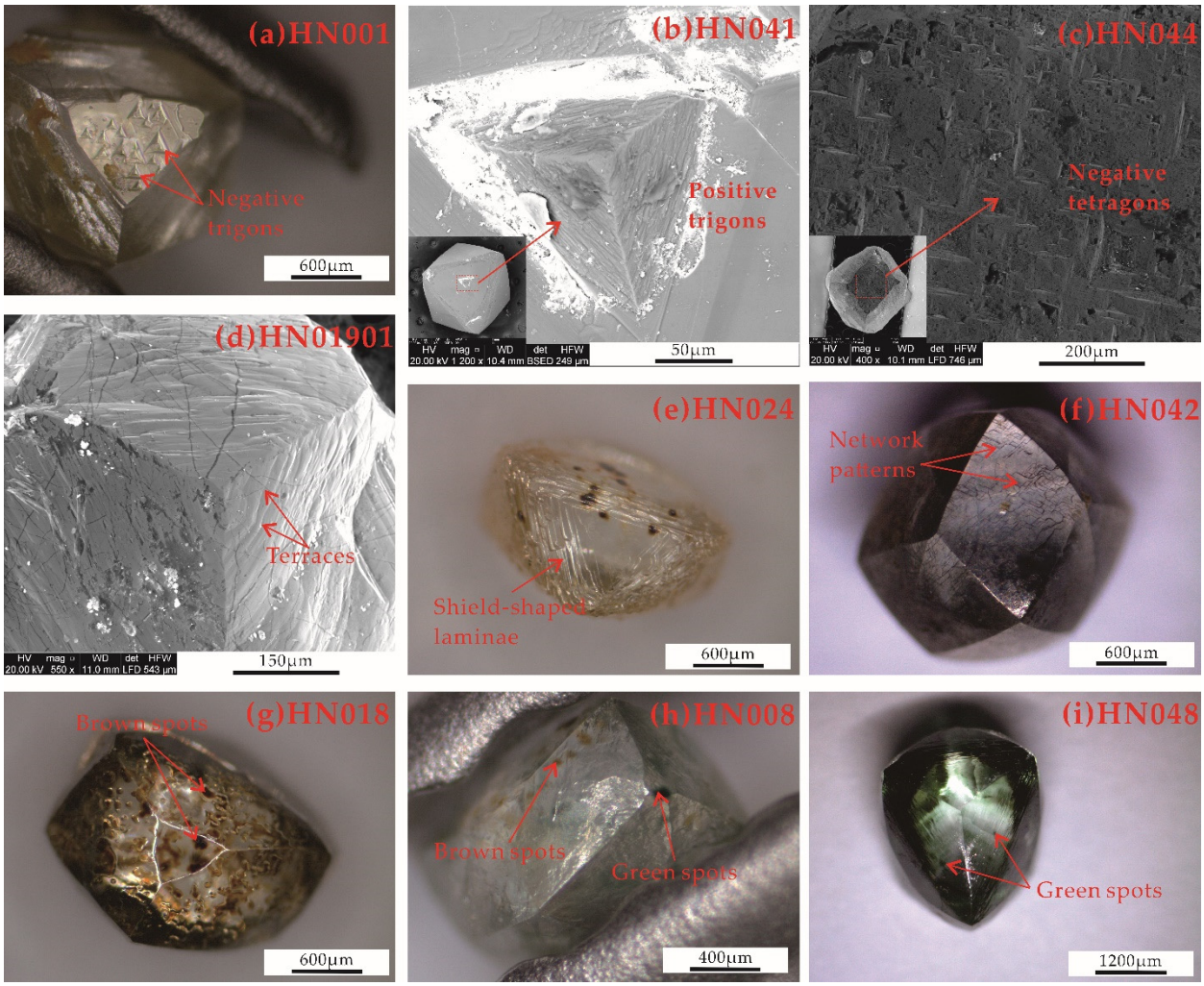

Figure 3. (**a**) Negative trigons; (**b**) Positive trigons; (**c**) Negative tetragons; (**d**) Terraces around the crystal apices of dodecahedra; (**e**) Shield-shaped laminae near the edges of octahedra; (**f**) Network patterns; (**g**) Brown surface spots; (**h**) Green spots and brown spots appearing on a dodecahedron diamond sample; (**i**) Green surface spots.

Terraces are extremely common on dodecahedron diamond samples. The size of each step usually varies between 10 to 40 μm. The existence of terracing results from the resorption process, which changes from octahedra to dodecahedra. The terraces can represent the exposed original octahedral growth planes in the diamond [35]. A dodecahedron diamond crystal that displays prominent terraces is likely to have been less resorbed than one displaying insignificant, or no, terraces [28].

4.1.4. Shield-Shaped Laminae

Shield-shaped laminae consist of superimposed laminae of progressively diminishing areal extent, and this structure was observed near the edges on all octahedral diamond samples (Figure 3e). Shield-shaped laminae are associated with resorption [28,30]. The outer laminae are exposed the soonest and recede the furthest, particularly from octahedral corners that are susceptible to resorption. As shield-shaped laminae develop throughout the diamond surface, this eventually leads to octahedral crystal edges being replaced by more curved dodecahedral surfaces [35].

4.1.5. Spots

Green and brown radiation stains are surface features usually identified in alluvial diamonds due to a diamond's proximity to radioactive fluids or minerals [36,37]. A total of 14 diamond samples had spots of faint to dark color on the surface.

Green surface spots are a common feature throughout the Hunan diamond population, which usually manifests as rounded-spot groups of about 20 μm to 80 μm in diameter (Figure 3i). These green-spot groups vary from faint to intense, leading to some diamonds with a light green-blue appearance.

Experiments have shown that green spots are generated by alpha-particle irradiation of the diamond surface when a radioactive mineral is adjacent. The formation of dark green spots requires about 10 Ma [37].

Brown surface spots are also a typical feature throughout the Hunan diamond population (Figure 3g). The intensity of color in the brown spots varies from faint to intense. The change in the color of spotting from green to brown is more likely to be a kinetic reaction that considers temperature and time, and not just temperature as thought before [33].

In the dodecahedron diamond sample HN008 (Figure 3h), the brown spots encountered are accompanied by superimposed or matching green spots. The occurrence of this matched pair may be explained by alpha-particle radiation hitting the diamond surface at some spots to generate a couple of green spots that, with time, changed to brown, followed by the diamond moving, inflecting radiation damage on a new adjacent area of the diamond surface [35].

4.1.6. Network Patterns

A crosswalk of highly curved, shallow ruts defines rhombic network patterns. Network patterns are observed on the dodecahedron surfaces of sample HN042, and the ruts tend to be narrow and shallow (Figure 3f).

Network patterns are typical in alluvial diamonds and rare or absent in diamonds collected directly from kimberlite/lamproite rocks [35,38]. In the Hunan alluvial diamonds, network patterns that post-date diamond resorption and etching occur with surface cracks, such as crescentic outline percussion marks. Surface cracks are produced by the transfer of kinetic energy when softer materials impact the diamond surface [29]. Thus, these are most likely the result of mechanical abrasion operating during diamond transportation.

4.2. FTIR Analysis

Diamonds are divided into two types (I and II) based on the presence or absence of nitrogen content; type I diamonds contain various forms of nitrogen and type II diamonds are considered to be nitrogen-free (possibly containing less than 20 ppm) [39].

Type I diamonds are further subdivided into type Ia and type Ib according to the aggregation of nitrogen atoms. In type Ia diamonds, two main forms of nitrogen aggregation are identified, namely A and B. Depending on the dominance of the A- or B-center, the type Ia diamond is classified as type IaA and type IaB, respectively [22,39]. Most natural diamonds from kimberlite or lamproite belong to the transitional type IaAB with both the A- and B-center [39]. Type II diamonds are further subdivided into type IIa and type IIb according to the occurrence of boron impurity. Type IIa has no significant absorption peak in the range of 1000~1400 cm^{-1}, while type IIb has an absorption peak caused by the B-C bond at 2800 cm^{-1}, representing the content of boron impurity in the diamond [39].

The studied diamond samples are of type IaAB and type IIa according to the spectral classification. A total of 34 diamond samples belong to the type IaAB, in which absorption peaks at 1282 cm^{-1} caused by the A-center and absorption peaks at 1175 cm^{-1} caused by the B-center appear simultaneously (e.g., Figure 4a). A total of seven diamond samples belong to type IIa (e.g., Figure 4b) without an absorption peak in the range of 1000–1400 cm^{-1} and 2800 cm^{-1}.

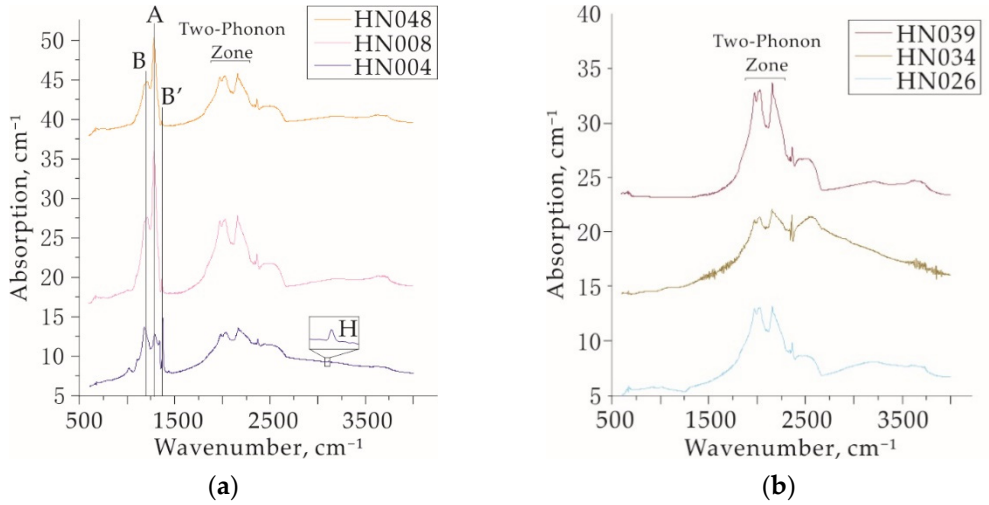

Figure 4. (**a**) IR absorption spectrum of representative type IaAB diamond samples: absorption peaks at 1282 cm^{-1} caused by A-center; absorption peaks at 1175 cm^{-1} caused by B-center; absorption peaks at 1360–1370 cm^{-1} caused by "Platelets" (B′-defects); and notice the absorption peak of H at 3107 cm^{-1} for sample HN004; (**b**) IR absorption spectrum of representative type IIa diamond samples.

The difference in the nitrogen content and aggregation state and the content of structural hydrogen in diamonds can be due to the different conditions of their formation, namely the pressure, temperature, and composition of the mineral-forming environment, so the content and state of nitrogen and hydrogen obtained from FTIR spectrometer are the most genetically informative parameters [19,40–44].

Table A1 presents the nitrogen contents and aggregation states, B′-defect (P) and structurally hydrogen (H) of the 34 studied type IaAB diamond samples.

4.2.1. Nitrogen Content and Aggregation States

N_A and N_B are the concentrations of A- and B-centers in terms of at. ppm, respectively. Groups of diamond crystals (populations) are similar in their distribution of nitrogen centers and contain one (main) or two (main and minor) diamond populations [42]. The distribution of the Hunan diamonds by the content of A-centers shows two pronounced peaks at ~150 and ~350 ppm (Figure 5a), which indicates two main populations of the Hunan diamonds. The proportion of aggregated nitrogen $\%B = 100 \times [N_B/(N_A + N_B)]$ in the diamond samples varies from 12% to 78% (Table A1). The distribution of %B model peaks at ~40% and ~70% (Figure 5b) can also be a sign of different primary sources of Hunan diamonds.

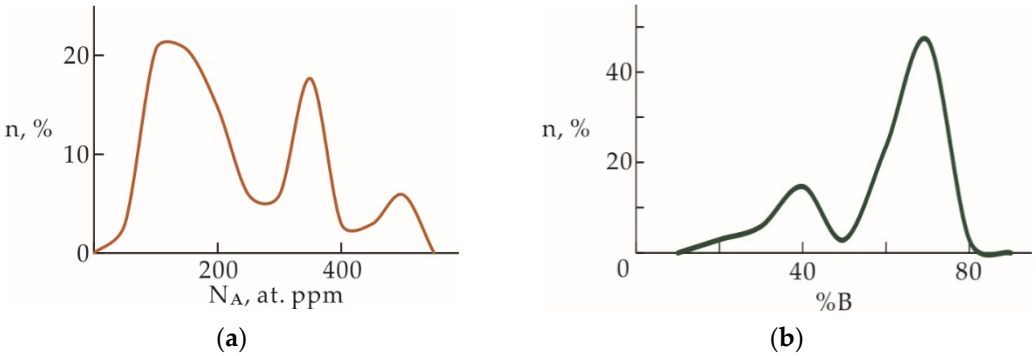

Figure 5. Nitrogen-content distribution of the Hunan diamonds: (**a**) By the contents of nitrogen A-centers; (**b**) By the extent of nitrogen aggregation (%B). n, diamond content in collections (%).

The total nitrogen content $N_{tot} = N_A + N_B$ of these diamond samples falls in the range of 196–1094 ppm (Table A1). Some localities (both kimberlites and placer deposits) are characterized by more than a single mode in the distribution of N_{tot} values in diamonds. A discussion about N_{tot} is a viable approach to identifying distinct populations in the deposits. The diamond crystals can be divided based on N_{tot} into three groups (Figure 6) [39]. Group 1 consists of low-nitrogen diamond crystals with N_{tot} ranging from almost 0–50 ppm. This group only includes diamonds from the Juina area in Brazil. It has minimal nitrogen content; by this criterion, the majority of the crystals are of type IIa with a variety of "super-deep diamond" [45,46]. Group 2 includes diamonds from the most famous diamond mines all over the world, such as the Yakutia pipes, Premier in South Africa, placers of Venezuela and the Coromandel area in Brazil, and the Hunan diamonds with total concentrations of the N_{tot} varying between 50 and 1000 ppm. Two subgroups may be distinguished among these samples. Group 2a has total concentrations of N_{tot} from 50 to 400 ppm, including diamonds from the famous Premier mine in South Africa, the Daldyn–Alakit kimberlite pipes in Yakutia, and the Arkhangelsk area in Russia. Group 2b, with a relatively higher N_{tot} (400–1000 ppm), includes diamonds from Hunan and all diamond deposits from Russia. Group 3 is high-nitrogen diamond crystals such as those from this study, the Arkhangelsk area, Triassic placer in NE Yakutia, Arkhangelsk area and placers of Urals in Russia, which contain between 1000 and 1700 ppm of N_{tot}.

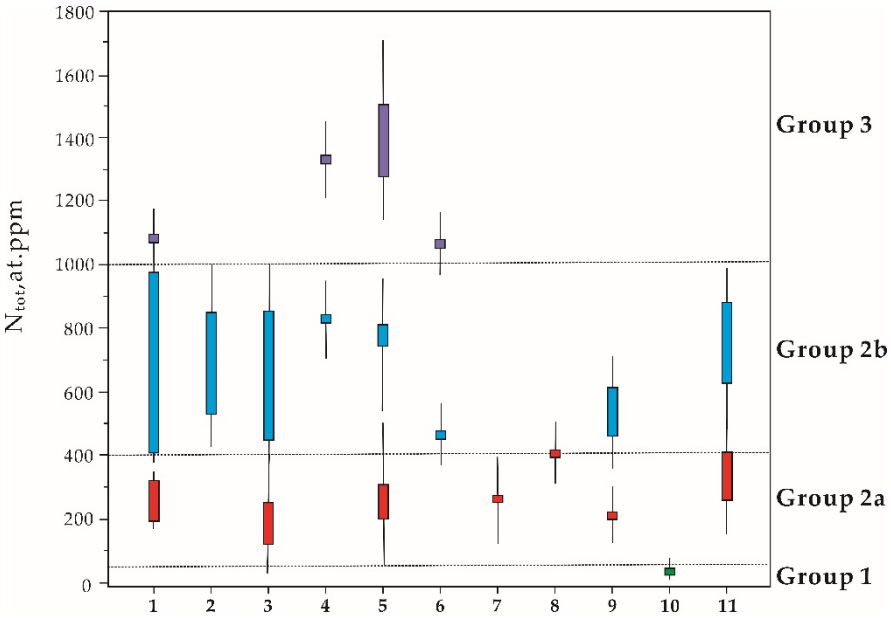

Figure 6. Ranges of variation in the content of structurally bound nitrogen (N_{tot}, at. ppm) in diamond crystals from different areas/placers. Solid columns: concentration ranges of N_{tot}; short lines: error range. Numbers on abscissa correspond to the area numbers: 1—Placer in the Yangtz Craton, China, this study; 2—Malo–Botuobiya area in Yakutia, Russia; 3—Daldyn–Alakit area of Yakutia, Russia; 4—Triassic placer in NE Yakutia, Russia; 5—Arkhangelsk area in Russia; 6—Placers of Urals, Russia; 7—Premier in South Africa; 8—DO-27 in Slave Province, Canada; 9—Coromandel area in Brazil; 10—Juina area in Brazil; 11—Placers of Venezuela. Modified by [39].

In general, each region is characterized by diamond crystals of one particular group [39,42]. However, consider the Arkhangelsk kimberlite province as an exception that has a remarkably similar N_{tot} distribution range to the Yuan River diamonds. Diamonds from the Arkhangelsk area in Russia belong to two groups, groups 2 and 3, due to diamonds from several local kimberlite pipes showing entirely different N_{tot} contents [39]. Considering the unknown-origin Hunan diamonds collected from the Yuan River in the vast area of the Yangtze Craton, the Hunan diamonds may be assumed as multi-source, similar to the Arkhangelsk area, in order to explain the wide range of N_{tot}.

4.2.2. Temperatures and Stages of Diamond Formation

The proportion of aggregated nitrogen in diamonds depends on the mantle residence temperature, age of the diamond, and the initial concentration of nitrogen [47]. There is no direct age study of Hunan diamonds inclusions such as garnet or zircon in previous research. Although both peridotitic-type and eclogitic-type inclusions were identified in Hunan diamonds [12], the number of inclusions remains too low for any statistical conclusion without any additional data on this study. An age of 3 Ga for the Hunan diamonds was assumed, as for most peridotitic diamonds worldwide [48]. In terms of N_{tot} and %B, most diamonds from the Yangtze Craton are similar to those from worldwide kimberlites, such as the major primary diamond deposits in Siberia (Daldyn-Alakit), Archangelsk area and South Africa [39,49]. These parameters indicate that the Yuan River diamonds formed at about 1075–1180 °C (Figure 7).

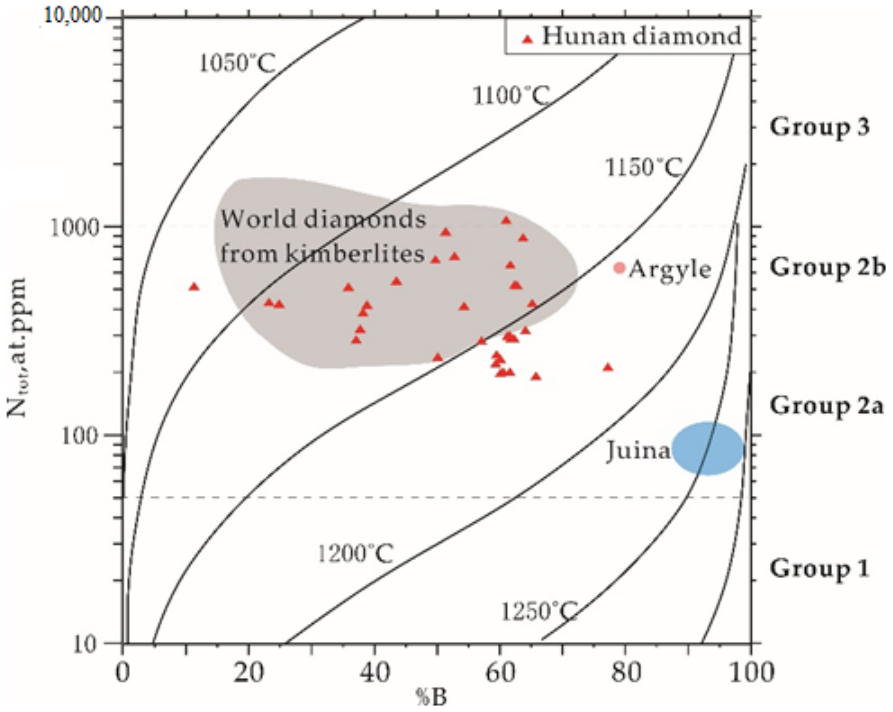

Figure 7. Nitrogen concentrations and aggregation in the Hunan diamond (red triangles) from the Yuan River basin alluvial deposits. Isotherm curves for 3 Ga are from [50], data on kimberlitic are from [51], data on lower-mantle diamonds are from [46], data on Argyle are from [52].

In comparison, diamonds from the classical lamproite-type Argyle mine have more aggregated nitrogen [52]. Approximately 10 Hunan diamond samples formed at slightly higher temperatures, overtaking the typical range of worldwide kimberlite diamonds and coming close to the Juina formation temperature of 1250 °C in the lower right-hand corner. The characteristic features of diamonds from the Juina area, Brazil, which are considered as typical lower-mantle diamonds due to an application of new mineralogical geothermometers for their super-deep mineral inclusions [53], are their almost 100% nitrogen aggregation [54] and extra low-nitrogen content. Comprehensive studies in the past have revealed occurrences of nitrogen-free (Type IIa) and low-nitrogen diamond crystals such as those from the Juina area are related to an ultramafic paragenesis [54]. In contrast, the eclogitic-type diamond is characterized by a higher nitrogen content [39]. Due to a considerable proportion of type IIa in Hunan diamonds and the higher temperature diamonds overtaking the typical kimberlite-diamond temperature range, an ultramafic paragenesis can also be a potential source of alluvial placer. Thus, the estimated temperature needs to be corrected when the actual age and new geothermometer mineral inclusions of diamonds from the Yangtze Craton are obtained.

4.2.3. Hydrogen and Platelets

The research on hydrogen centers (H) and the conditions of their formation is significative as it provides insight into mantle fluids [32,55]. Hydrogen is one of the reducing agents for carbon dioxide during diamond growth in carbonate–silicate systems. The amount of structural hydrogen is determined by the crystal-growth mechanism, which depends on the conditions of diamond formation [55].

Hydrogen can be present not only as structural defects in the lattice but also as -OH groups and H_2O in diamond micro-inclusions [56,57]. In addition, the hydrogen in many diamonds is not IR-active hydrogen (inactive state of some hydrogen-containing defects in the IR region), so the hydrogen content in diamonds is difficult to quantify.

Platelets (P, interstitial plane B′-defects in the cube plane {100}) form during nitrogen accumulation in diamonds in conjunction with the formation of nitrogen B-centers [58–60]. Platelets and hydrogen centers, like nitrogen defects, are also important indicators of formation conditions.

All the studied samples were low in hydrogen. A total of 22 pieces of Type IaAB diamonds had hydrogen absorption peaks while the absorption coefficient α_{3107}(H) varied between 0.03–4.67 cm^{-1}, and most of the α_{3107}(H) < 1 cm^{-1} (Table A1), and only two samples, number HN009 (α_{3107}(H) ≈ 2.95 cm^{-1}) and HN047 (α_{3107}(H) ≈ 4.68 cm^{-1}), having absorption coefficients > 1 cm^{-1}.

The studied alluvial diamonds from the Yangtze Craton were similar in terms of their low contents of hydrogen (usually <1 cm^{-1}) (Figure 8 and Table A1) to some diamond groups with low hydrogen content from the Ural placers [21], the Juina placers, and the super-deep diamonds of kimberlite pipes in Brazil [39]. The intensity of the hydrogen correlation peak increases with increasing nitrogen content, and this correlation is more dramatically reflected in Figure 8, where the hydrogen-correlation-peak coefficient is presented as a logarithm on a base of 10. The diamond samples with different morphology both showed this same tendency, indicating that the correlation is not sensitive to the nitrogen form. A similar correlation of nitrogen and hydrogen has also been observed in diamonds from the Argyle mine [52].

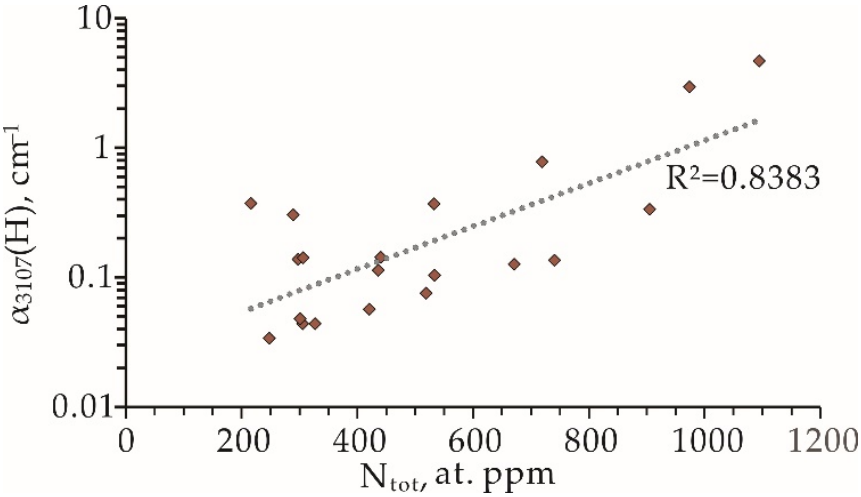

Figure 8. The integrated absorption of the α_{3107}(H) vs. the concentration of total nitrogen content (N_{tot}) in the studied Hunan diamonds. The dotted line points to a possible correlation with R^2 = 0.8383.

The diamond samples were all relatively poor in platelets, with 29 type IaAB diamond samples having platelet absorption peaks. The concentration of platelets in the diamonds (absorption coefficient α(B′)) fell in the range 0.23–17 cm^{-1}, with most concentrated below 2 cm^{-1} and only four samples with absorption peaks greater than 2 cm^{-1}.

The Hunan diamond samples from the Yuan River Basin showed at least two main populations via the statistics evidence from N_A, N_{tot} and aggregated nitrogen %B. Plac-

ers include more than two populations, which might be due to the abundance of their primary sources, each characterized by the particular geochemical and P-T conditions of the formation and post-crystallization annealing of diamonds. By comparing the states with other diamond pipes or placers, the Hunan diamonds still showed unusual FTIR characteristics: significant peaks in the distribution model of N_A and %B, a wide range of N_{tot}, and some samples of higher formation temperature than classical kimberlite-type diamonds. Therefore, in prospecting diamond-deposit exploration at the Yuan River basin, multi-source primary host rocks should be of attention, including kimberlite/lamproite and ultramafic rocks.

5. Conclusions

Most Hunan diamonds are monocrystal forms. The common monocrystal forms observed in Hunan diamond samples were octahedral, THH and dodecahedra. Additionally, some samples also exhibited octahedral–rhom-dodecahedral transitional behaviors and irregular forms. Trigons and tetragons, terraces and shield-shaped laminae, as frequent surface features in Hunan diamonds, result from dissolution and reabsorption in the mantle and magma. Green and brown spots that changed the color of the diamond surface are caused by irradiation, indicating that alluvial diamonds have been deposited for a long time. Network patterns and other mechanical abrasion marks are typical of Hunan alluvial diamonds.

The main types of alluvial Hunan diamonds from the Yangtze Craton are type IaAB and type IIa. Type IaAB Hunan diamond samples have a wide range of total nitrogen content from 196–1094 ppm, with the nitrogen content in the A-center mainly concentrated at ~150 and ~350 ppm, and the degree of nitrogen aggregation %B varying over a wide range, but mainly at ~40% and ~70%. So, at least two populations exist in Yuan River basin alluvial-diamond placer. Hunan diamonds are low in structural hydrogen and platelets. The platelet-absorption coefficient varied in the range of 0.23–17 cm^{-1}, and most were concentrated below 2 cm^{-1}. The samples' hydrogen-absorption coefficient varied between 0.03–4.67 cm^{-1}, and most of the $\alpha_{3107}(H) < 1$ cm^{-1}, similar to the low-hydrogen-content diamonds from the Ural placers, the Juina placers, and the super-deep diamonds of the kimberlite pipes in Brazil. Moreover, there is a significant positive correlation between hydrogen correlation peak and total nitrogen content, which has also been observed in the Argyle diamond deposit.

Assuming an age of 3 Ga for Hunan diamonds, they formed at about 1075–1180 °C, mainly conforming to the kimberlite diamond range. Besides, some samples with slightly higher temperatures were close to the ultramafic-related Juina diamonds. The analysis and comparison of FTIR characteristics indicate that multiple sources of Hunan diamonds should be considered.

Author Contributions: Data curation, C.C. and Y.W.; materials, F.Z.; writing—original draft preparation, C.C.; writing—review and editing, F.L.; visualization, C.C. and S.Y.; supervision, J.Y.; project administration, J.Y.; funding acquisition, J.Y. All authors have read and agreed to the published version of the manuscript.

Funding: This research was funded by the National Natural Science Foundation of China (No. 41720104009 and 92062215).

Data Availability Statement: Not applicable.

Acknowledgments: We thank three anonymous referees and Editors for their helpful comments which greatly helped in improving our paper. We gratefully acknowledge Ye Yuan and Jiaxin Wan for help with FTIR tests; Xiaomin Wang for help in SEM imaging. We thank Dongyang Lian and Weiwei Wu for their valuable discussions.

Conflicts of Interest: The authors declare no conflict of interest.

Appendix A

Table A1. Evaluation of nitrogen and hydrogen defects in type IaAB Hunan diamonds by FTIR.

Sample	Weight/mg	N_A	N_B	N_{tot}	%B	α (B′)	α_{3107} (H)
HN001	19.5	253	417	671	62	6.06	0.13
HN002	24.5	346	394	740	53	1.11	0.14
HN003	26	119	123	241	51	0.55	null
HN004	7.5	151	289	441	66	6.86	0.14
HN005	11	248	156	405	39	0.95	null
HN006	8	93	143	236	61	null	null
HN007	13.3	77	127	204	62	null	null
HN008	7	336	104	440	24	1.97	null
HN009	3	469	505	974	52	1.88	2.95
HN010	15	185	112	297	38	0.63	null
HN011	28.4	203	125	329	38	1.55	null
HN012	3.2	116	211	326	65	0.44	0.04
HN013	1.1	116	190	305	62	0.56	0.04
HN016	20.1	198	335	533	63	8.94	0.37
HN017	5.3	114	187	300	62	0.37	0.05
HN018	13	315	247	562	44	1.89	null
HN019	1.2	191	229	420	55	0.29	0.06
HN020	6	80	123	203	61	null	null
HN021	20	99	148	247	60	0.23	0.03
HN022	17.6	324	581	905	64	17.12	0.33
HN023	1.3	467	61	529	12	0.70	null
HN024	9.4	331	187	518	36	4.15	0.08
HN032	16	66	130	196	66	null	0.60
HN033	31.4	80	126	206	61	null	0.18
HN036	31	111	187	298	63	0.38	0.14
HN037	20.6	91	135	226	60	0.37	null
HN040	61.6	117	189	306	62	0.88	0.14
HN041	6	326	110	435	25	1.45	0.11
HN042	17.8	196	338	533	63	1.97	0.10
HN043	13.8	122	166	289	58	0.92	0.30
HN045	6.3	357	361	718	50	0.67	0.78
HN046	3.8	48	168	216	78	0.32	0.37
HN047	4	421	673	1094	61	2.99	4.68
HN048	42.1	261	168	428	39	0.69	null

Nitrogen content of the error range is about 15%.

References

1. Stachel, T.; Harris, J.W. The origin of cratonic diamonds—Constraints from mineral inclusions. *Ore Geol. Rev.* **2008**, *34*, 5–32. [CrossRef]
2. Woods, G.S.; Collins, A.T. Infrared absorption spectra of hydrogen complexes in type I diamonds. *J. Phys. Chem. Solids* **1983**, *44*, 471–475. [CrossRef]
3. Boyd, S.R.; Mattey, D.P. Multiple growth events during diamond genesis: An integrated study of carbon and nitrogen isotopes and nitrogen aggregation state in coated stones. *Earth Planet. Sci. Lett.* **1987**, *86*, 341–353. [CrossRef]
4. Boyd, S.R.; Kiflawi, I. The relationship between infrared absorption and the A defect concentration in diamond. *Philos. Mag. B Phys. Condens. Matter.* **1994**, *69*, 1149–1153. [CrossRef]
5. Boyd, S.R.; Woods, I.K. Infrared absorption by the B nitrogen aggregate in diamond. *Philos. Mag. B Phys. Condens. Matter.* **1995**, *72*, 351–361. [CrossRef]
6. Mendelssohn, M.J.; Milledge, H.J. Geologically Significant Information from Routine Analysis of the Mid-Infrared Spectra of Diamonds. *Int. Geol. Rev.* **1995**, *37*, 95–110. [CrossRef]
7. Fedortchouk, Y.; Canil, D. Mechanisms of diamond oxidation and their bearing on the fluid composition in kimberlite magmas. *Am. Mineral.* **2007**, *92*, 1200–1212. [CrossRef]
8. Fedortchouk, Y.; Matveev, S. H_2O and CO_2 in kimberlitic fluid as recorded by diamonds and olivines in several Ekati Diamond Mine kimberlites, Northwest Territories, Canada. *Earth Planet. Sci. Lett.* **2010**, *289*, 549–559. [CrossRef]
9. Fedortchouk, Y.; Liebske, C. Diamond destruction and growth during mantle metasomatism: An experimental study of diamond resorption features. *Earth Planet. Sci. Lett.* **2019**, *506*, 493–506. [CrossRef]

10. Afanasiev, V.P.; Pokhilenko, N.P. *Wear of Diamond: An Experimental Study and Field Evidence, Proceedings of 10th International Kimberlite Conference, Bangalore, India, 5–11 February 2012*; Pearson, D.G., Grütter, H.S., Harris, J.W., Kjarsgaard, B.A., O'Brien, H., Rao, N.V.C., Sparks, S., Eds.; Springer: New Delhi, India, 2013; Volume 1, pp. 324–328.
11. Ma, W. Characteristics of the jew grade placer diamond deposit in Yuanjiang River valley. *Hunan Geol.* **1989**, *8*, 51–53. (In Chinese)
12. Ma, Y.; Qiu, Z. Geochemical characteristics of fluvial detrital garnet in Chenxi area of Yuan River and its enlightenment to primary Hunan diamond prospecting. *Acta Petrol. Miner.* **2021**, *40*, 15. (In Chinese)
13. Zhao, T.; Zhu, G. Evidence for discrete Archean microcontinents in the Yangtze Craton. *Precambr. Res.* **2021**, *361*, 106259. [CrossRef]
14. Zhao, G.; Cawood, P.A. Amalgamation of the North China Craton: Key issues and discussion. *Precambr. Res.* **2012**, *222–223*, 55–76. [CrossRef]
15. Zhang, S.; Zheng, Y. Zircon U-Pb age and Hf-O isotope evidence for Paleoproterozoic metamorphic event in South China. *Precambr. Res.* **2006**, *151*, 265–288. [CrossRef]
16. Li, W.; Shi, Z. Origin and tectonic implications of the early Middle Triassic tuffs in the western Yangtze Craton: Insight into whole-rock geochemical and zircon U-Pb and Hf isotopic signatures. *Gondwana Res.* **2021**, *93*, 142–161. [CrossRef]
17. Huang, Y.; Li, Z. Mineralogical characteristics of primary and placer diamonds of potassium-magnesium lamprophyre in Zhenyuan, Guizhou Province and their prospecting significance. *Acta Sci. Nat. Univ. Sunyatseni* **2016**, *55*, 11. (In Chinese)
18. Yang, X.; Cai, Y. Discovery of diamond-bearing tuffaceous facies in Ligonggang area, Taoyuan, Hunan and its prospecting significance. *Geol. Surv. China* **2019**, *6*, 56–62. (In Chinese)
19. Bokii, G.B.; Bezrukov, G.N. *Natural and Synthetic Diamonds*; Nauka Press: Moscow, Russia, 1986. (In Russian)
20. Khachatryan, G.K. *Improved Methods of Evaluating Nitrogen Concentration in Diamond and its Practical Application*; Geological Material Base ALROSA: Mirny, Russia, 2003; pp. 319–321. (In Russian)
21. Fedorova, E.N.; Logvinova, A.M. Typomorphic characteristics of the Ural diamonds (from FTIR spectroscopy data). *Russ. Geol. Geophys.* **2013**, *54*, 1458–1470. [CrossRef]
22. Davies, G. Decomposing the IR absorption spectra of diamonds. *Nature* **1981**, *290*, 40–41. [CrossRef]
23. Howell, D.; O'Neill, C.J. μ-FTIR mapping: Distribution of impurities in different types of diamond growth. *Diam. Relat. Mater.* **2012**, *29*, 29–36. [CrossRef]
24. Harlow, G.E.; Davies, R.M. Diamonds. *Elements* **2005**, *1*, 67–70. [CrossRef]
25. Tappert, R.; Tappert, M.C. *Diamonds in Nature. A Guide to Rough Diamonds*; Springer: Berlin/Heidelberg, Germany, 2011; p. 142.
26. Khokhryakov, A.; Pal'yanov, Y. Influence of the fluid composition on diamond dissolution forms in carbonate melts. *Am. Mineral.* **2010**, *95*, 1508–1514. [CrossRef]
27. Fedortchouk, Y. A new approach to understanding diamond surface features based on a review of experimental and natural diamond studies. *Earth-Sci. Rev.* **2019**, *193*, 45–65. [CrossRef]
28. Robinson, D.N. Surface Textures and Other Features of Diamonds. Ph.D. Thesis, The University of Cape Town, Cape Town, South Africa, 1979.
29. Wilks, E.; Wilks, J. *Properties and Applications of Diamond*; Butterworth Heinemann: Oxford, UK, 1994; p. 525.
30. Zhang, Z.; Fedortchouk, Y. Records of mantle metasomatism in the morphology of diamonds from the Slave craton. *Eur. J. Mineral.* **2012**, *24*, 619–632. [CrossRef]
31. Sunagawa, I. Morphology of natural and synthetic diamond crystals. In *Materials Science of the Earth's Interior*; Sunagawa, I., Ed.; Terra Scientific Publishing: Tokyo, Japan, 1984; pp. 303–330.
32. Mendelssohn, M.J.; Milledge, H.J. Morphological characteristics of diamond populations and relation to temperature-dependent growth and dissolution rates. *Int. Geol. Rev.* **1995**, *37*, 285–312. [CrossRef]
33. Harris, J.W. Diamond Geology. In *The Properties of Natural and Synthetic Diamond*; Field, J.E., Ed.; Academic Press: London, UK, 1992; pp. 345–393.
34. Li, Z.; Fedortchouk, Y. Positively oriented trigons on diamonds from the Snap Lake kimberlite dike, Canada: Implications for fluids and kimberlite cooling rates. *Am. Mineral.* **2018**, *103*, 1634–1648. [CrossRef]
35. Laiginhas, F. Diamond from the Ural Mountains: Their Characteristics and the Mineralogy and Geochemistry of Their Inclusions. Ph.D. Thesis, University of Glasgow, Glasgow, UK, 2008.
36. Smit, K.V.; Shirey, S.B. Diamonds Are Not Forever! Diamond Dissolution. *Gems Gemol.* **2020**, *56*, 148–155.
37. Vance, E.R.; Milledge, H.J. Natural and laboratory alpha-particle irradiation of diamond. *Mineral. Mag.* **1972**, *38*, 878–881. [CrossRef]
38. Orlov, Y.L. *The Mineralogy of the Diamond*; John Wiley and Sons: New York, NY, USA, 1977; p. 235.
39. Kaminsky, F.V.; Khachatryan, G.K. Characteristics of nitrogen and other impurities in diamond, as revealed by infrared absorption data. *Can. Mineral.* **2001**, *39*, 1733–1745. [CrossRef]
40. Logvinova, A.M.; Wirth, R. The phase composition of crystal-fluid nanoinclusions in alluvial diamonds in the northeastern Siberian Platform. *Russ. Geol. Geophys.* **2011**, *52*, 1286–1297. [CrossRef]
41. Zedgenizov, D.A.; Ragozin, A.L.; Shatsky, V.S.; Araujo, D.; Griffin, W.L. Fibrous diamonds from the placers of the northeastern Siberian Platform: Carbonate and silicate crystallization media. *Russ. Geol. Geophys.* **2011**, *52*, 1298–1309. [CrossRef]
42. Khachatryan, G.K.; Kaminsky, F.V. "Equilibrium" and "non-equilibrium" diamond crystals from deposits in the east European platform, as revealed by infrared absorption data. *Can. Mineral.* **2003**, *41*, 171–184. [CrossRef]
43. Khachatryan, G.K.; Zinchuk, N.N. Study of optically active centers in diamonds from Uralian placers: An attempt to locate their primary deposits. *Russ. Geol. Geophys.* **2004**, *45*, 226–234.

44. Palot, M.; Cartigny, P. Diamond origin and genesis: A C and N stable isotope study on diamonds from a single eclogitic xenolith (Kaalvallei, South Africa). *Lithos* **2009**, *112S*, 758–766. [CrossRef]
45. Kaminsky, F.V.; Zakharchenko, O.D. Superdeep diamonds from the Juina area, Mato Grosso State, Brazil. *Contrib. Mineral. Petrol.* **2001**, *140*, 734–753. [CrossRef]
46. Kaminsky, F.V. (Ed.) Diamond in the Lower Mantle. In *The Earth's Lower Mantle: Composition and Structure*; Springer: Berlin, Germany, 2017; pp. 229–257.
47. Evans, T. Aggregation of nitrogen in diamond. In *The Properties of Natural and Synthetic Diamond*; Field, J.E., Ed.; Academic Press: London, UK, 1992; pp. 259–290.
48. Shirey, S.B.; Richardson, S.H. Age, paragenesis and composition of diamonds and evolution of the Precambrian mantle lithosphere of southern Africa. *S. Afr. J. Geol.* **2004**, *107*, 91–106. [CrossRef]
49. Mainkar, D.; Gupta, T. *Diamonds from the Behradih Kimberlite Pipe, Bastar Craton, India: A Reconnaissance Study, Proceedings of 10th International Kimberlite Conference, Bangalore, India, 5–11 February 2012*; Pearson, D.G., Grütter, H.S., Harris, J.W., Kjarsgaard, B.A., O'Brien, H., Rao, N.V.C., Sparks, S., Eds.; Springer: New Delhi, India, 2013; Volume 1, p. 314.
50. Taylor, W.R.; Milledge, H.J. Nitrogen aggregation character, thermal history and stable isotope composition of some xenolith–derived diamonds from Roberts Victor and Finch. In *Extended Abstracts, Proceedings of the Sixth International Kimberlite Conference, Novosibirsk, Russia, 1–18 August 1995*; United Institute of Geology, Geophysics and Mineralology, Siberian Branch of Russian Academy of Sciences: Novosibirsk, Russia, 1995; pp. 620–622.
51. Kvasnytsya, V.M.; Kaminsky, F.V. Unusual green Type Ib–Iab Dniester-type diamond from Ukrainian placers. *Mineral. Petrol.* **2021**, *115*, 149–160. [CrossRef]
52. Iakoubovskii, K.; Adriaenssens, G.J. Optical characterization of natural Argyle diamonds. *Diam. Relat. Mater.* **2002**, *11*, 125–131. [CrossRef]
53. Kaminsky, F. Earth-Science Reviews Mineralogy of the lower mantle: A review of 'super-deep' mineral inclusions in diamond. *Earth Sci. Rev.* **2012**, *110*, 127–147. [CrossRef]
54. Araujo, D.P.; Gaspar, J.C. *Juina Diamonds from Kimberlites and Alluvials: A Comparison of Morphology, Spectral Characteristics and Carbon Isotope Composition, Proceedings of 10th International Kimberlite Conference, Bangalore, India, 5–11 February 2012*; Pearson, D.G., Grütter, H.S., Harris, J.W., Kjarsgaard, B.A., O'Brien, H., Rao, N.V.C., Sparks, S., Eds.; Springer: New Delhi, India, 2013; Volume 1, pp. 255–269. [CrossRef]
55. Pal'yanov, Y.N.; Sokol, A.G. Conditions of diamond formation through carbonate–silicate interaction. *Eur. J. Mineral.* **2005**, *17*, 207–214. [CrossRef]
56. Tschauner, O.; Huang, S. Ice-VII inclusions in diamonds: Evidence for aqueous fluid in Earth's deep mantle. *Science* **2018**, *359*, 1136–1139. [CrossRef] [PubMed]
57. Kagi, H.; Lu, R.; Davidson, P. Evidence for ice VI as an inclusion in cuboid diamonds from high P-T near infrared spectroscopy. *Mineral. Mag.* **2000**, *64*, 1089–1097. [CrossRef]
58. Goss, J.P.; Coomer, B.J. Extended defects in diamond: The interstitial platelet. *Phys. Rev. B.* **2003**, *67*, 165208. [CrossRef]
59. Sobolev, E.V.; Lisoivan, V.I. Platy formations in the structure of natural diamonds. *Zh. Strukturnoi Khimii* **1968**, *9*, 1029–1033.
60. Woods, G.S. Platelets and the infrared absorption of type Ia diamonds. *Proc. R. Soc. Lond. Ser. A* **1986**, *407*, 219–238.